Glycobiology, 2023, **33**, 9, 715–731
https://doi.org/10.1093/glycob/cwad044
Advance access publication date 8 June 2023
Original Article

Direct antitumoral effects of sulfated fucans isolated from echinoderms: a possible role of neuropilin-1/β1 integrin endocytosis and focal adhesion kinase degradation

Antonio G.F. Lima[1,2,†], Viviane W. Mignone[1,†], Francisco Vardiero[1], Eliene O. Kozlowski[2,‡], Laila R. Fernandes[1], Juliana M. Motta[2], Mauro S.G. Pavão[2], Camila C. Figueiredo[1], Paulo A.S. Mourão[2], Verônica Morandi[1,*]

[1]Laboratório de Biologia da Célula Endotelial e da Angiogênese (LabAngio), Departamento de Biologia Celular/IBRAG, Universidade do Estado do Rio de Janeiro (UERJ), Rio de Janeiro, 20550-013, Brazil, [2]Laboratório do Tecido Conjuntivo, Instituto de Bioquímica Médica (IBqM) - Universidade Federal do Rio de Janeiro (UFRJ), Hospital Universitário Clementino Fraga Filho, Rio de Janeiro, 21941-913, Brazil

*Corresponding author: Department of Cell Biology/LabAngio Rua São Francisco Xavier, Universidade do Estado do Rio de Janeiro (UERJ), 524—PHLC Labs 203/204 Maracanã, Rio de Janeiro, RJ 20550-013, Brazil. E-mail: veronica@uerj.br

†These authors equally contributed to this work.
‡In memoriam.

Hypercoagulability, a major complication of metastatic cancers, has usually been treated with heparins from natural sources, or with their synthetic derivatives, which are under intense investigation in clinical oncology. However, the use of heparin has been challenging for patients with risk of severe bleeding. While the systemic administration of heparins, in preclinical models, has shown primarily attenuating effects on metastasis, their direct effect on established solid tumors has generated contradictory outcomes. We investigated the direct antitumoral properties of two sulfated fucans isolated from marine echinoderms, FucSulf1 and FucSulf2, which exhibit anticoagulant activity with mild hemorrhagic potential. Unlike heparin, sulfated fucans significantly inhibited tumor cell proliferation (by ~30–50%), and inhibited tumor migration and invasion in vitro. We found that FucSulf1 and FucSulf2 interacted with fibronectin as efficiently as heparin, leading to loss of prostate cancer and melanoma cell spreading. The sulfated fucans increased the endocytosis of β1 integrin and neuropilin-1 chains, two cell receptors implicated in fibronectin-dependent adhesion. The treatment of cancer cells with both sulfated fucans, but not with heparin, also triggered intracellular focal adhesion kinase (FAK) degradation, with a consequent overall decrease in activated focal adhesion kinase levels. Finally, only sulfated fucans inhibited the growth of B16-F10 melanoma cells implanted in the dermis of syngeneic C57/BL6 mice. FucSulf1 and FucSulf2 arise from this study as candidates for the design of possible alternatives to long-term treatments of cancer patients with heparins, with the advantage of also controlling local growth and invasion of malignant cells.

Key words: cancer; FAK; fibronectin; integrin endocytosis; sulfated polysaccharides.

Introduction

Adhesion, proliferation, and migration are crucial cellular steps for cancer progression and metastasis (Hanahan and Weinberg 2011; Sosa et al. 2014). Common complications of metastatic cancer, a major responsible for poor prognosis and death in most patients, are venous thromboembolism and arterial thrombosis, which strongly correlate with fatal outcome (Razak et al. 2018). Heparin, a sulfated polysaccharide from the glycosaminoglycans family, and its derivatives have been under intense investigation in clinical oncology, initially for the need to treat cancer patients for blood hypercoagulability. Some studies have suggested that it reduces the emergence of metastatic lesions and prolongs survival in cancer patients (Kuderer et al. 2007; Ma et al. 2020). Heparin is mostly available from porcine intestine and occurs either as crude unfractionated heparin (UFH) or in fractionated low-molecular-weight heparin forms (LMWH). LMWH are generated by different depolymerization methods, thus products bearing variable chemical and biological properties are obtained (Atallah et al. 2020).

Most of heparin antitumor properties seems to take place independently of its potent anticlotting activity (Casu et al. 2008), especially by its ability to inhibit tumor interactions with other cells. By interfering with P- and L-selectins, and VLA4-integrin-dependent cell–cell adhesion, heparin inhibits the interaction of tumor cells with both platelets and the endothelium, during hematogenous metastasis (Bendas and Borsig 2012). The inhibition of heparanases, which have been implicated in breaking down the extracellular matrix (ECM) during cell migration (Bendas and Borsig 2020), and the blockage of the angiogenic signaling pathways, through sequestering of growth factors (e.g. FGFs and VEGFs) away from their low-affinity surface heparan sulfate proteoglycan (HSPG) receptors (Xie and Li 2019), have also been pointed out as possible therapeutic targets for heparin.

Despite these functional properties, the use of heparin in cancer therapy has been restricted, or even challenging for those patients with a high risk of severe bleeding (Lee and Peterson 2013). Another layer of complexity is represented by the fact that the currently available studies have raised

Received: September 29, 2022. **Revised:** May 30, 2023. **Accepted:** May 30, 2023

contradictory data on whether heparin exerts direct effects on tumor cell proliferation and migration, two important skills leading to sustained growth and invasion in established tumors, not only at primary sites but also at metastatic foci (Disanza et al. 2019). Therefore, the search for new anticoagulant agents that could exert direct antitumor effects but with reduced hemorrhagic risk has stimulated the design of synthetic heparin mimetics (Gockel et al. 2021), as well as the identification of new bioactive sulfated polysaccharides from other natural sources.

Sulfated fucans from seaweeds (fucoidans) can also interfere in coagulation, tumor growth and metastasis, usually mimicking the effects of heparin (Pomin and Mourão 2014), but the heterogeneity and complexity of their molecular structures make it hard to fully decipher their biochemical properties (Pereira et al. 1999), thus limiting the establishment of consistent structure–function correlations. On the other hand, sulfated fucans from echinoderms have simple, unique structures of linear chains of α-L-fucose in well-defined repetitive patterns (Mulloy et al. 1994; Ribeiro et al. 1994; Alves et al. 1997). Based on their specific sulfation patterns, positioning of glycosidic bonds (which vary within species), and their low anticoagulant potential (as compared with heparins) that resembles that of mammalian dermatan sulfate (Pereira et al. 1999), we hypothesized that sulfated fucans from echinoderms could also functionally diverge from heparin when evaluated in the context of tumor growth, adhesion, and migration.

In this work, we investigated two sulfated fucans isolated from echinoderms, for their direct on the proliferation, adhesion, and migration of different tumor cell lines (from both carcinoma and non-carcinoma phenotypes). We also compared their effect to those observed with heparin. As shown in Fig. 1A, both polysaccharides are composed of α-L-fucopyranosyl units. While FucSulf1, extracted from the sea urchin *Lytechinus variegatus* (Echinoidea), and FucSulf2, isolated from the sea cucumber *Holothuria grisea* (Holothuroidea), share the same [1 → 3] glycosidic bonding, they exhibit slightly different sulfation patterns, in which the 4 residues of the tetrasaccharide repeating units differ only by specific patterns of sulfation at the O-2 and O-4 positions (Pereira et al. 1999; Glauser et al. 2013).

Our results show that the sulfated fucans isolated from *L. variegatus* and *H. grisea* are potential antitumor agents that may represent viable alternatives to heparin in cancer therapy, possibly by acting through multifaceted anti-adhesive mechanisms.

Results

FucSulf1 delays tumor cell proliferation in vitro

We first investigated the direct effect of FucSulf1, the sulfated fucan purified from *L. variegatus*, on tumor cell proliferation. An initial FucSulf1 concentration range was estimated from cell-based observations already published by our group on the effect of sulfated polysaccharides in cancer cells (Borsig et al. 2007), in the blood coagulation process (Fonseca et al. 2010), or from our unpublished data on endothelial cell tubulogenesis (IC_{50} varying from 3.5 to 50 μg/mL, for sulfated polysaccharides isolated from 3 different species of echinoderms—not shown). In a pilot experiment using PC-3 cells (a prostate carcinoma cell line from grade IV adenocarcinoma, with high metastatic potential, Namekawa et al. 2019) treated with growing concentrations of 1, 10, and 100 μg/mL of FucSulf1 (Fig. 1B), we found that FucSulf1 significantly delayed (by ~30%) tumor proliferation at 100 μg/mL, after 48 h of treatment. We kept the concentration of 100 μg/mL in subsequent experiments.

The possibility that FucSulf1 could exert broad cytotoxic effects was ruled out after the evaluation of cell viability by flow cytometry analysis (Fig. 1C), using the annexin V/propidium iodide double-staining method. We also evaluated a second prostate cancer cell line, DU-145 (with moderated metastatic potential) (Braicu et al. 2019). The number of viable cells, represented by the cell populations in the lower left quadrants in each panel (surrounded by dashed green lines), was not significantly affected by the incubation of DU-145 cells (75.7% ± 9.5 in treated cells, versus 76.3% ± 8.2 observed in untreated cells) and PC-3 cells (80.5% ± 8.8 versus 84.2% ± 7.4) with FucSulf1, suggesting that this sulfated fucan exerted a cytostatic, rather than a cytotoxic effect on tumor growth.

FucSulf1—but not heparin—inhibited the proliferation of cells DU-145 and PC-3 cells at 100 μg/mL (by ~35 and 30% of inhibition after 72 h of incubation, respectively) (Fig. 1D). Interestingly, it was also able to decrease the proliferation of another carcinoma-type cell line, the highly metastatic MDA-MB-231 breast cancer cells after 24 h (~34% inhibition), but the effect was less sustainable over time (only ~12% inhibition, after 48 h), when compared with the prostate carcinoma cell lines.

The activation status of some major signaling pathways related to cell proliferation and survival, such as mitogen-activated protein kinases (MAPKs) ERK1/2 and p38-MAPK, besides protein kinase B/Akt (PKB/Akt) was also studied (Manning and Toker 2017; Braicu et al. 2019). PKB/Akt was not inhibited by FucSulf1 (Fig. S1A), in the standard condition of our proliferation assays (non-starved DU-145 and PC-3 cells, grown in the presence of 5% serum). To check whether the cell lines were responsive to growth factors in more stringent conditions, we evaluated the effect of FucSulf1 on the activity of ERK1/2 (Fig. S1B) and p38 MAPK (Fig. S1C) when DU-145 and PC-3 cells were challenged with purified growth factors (FGF-2 and EGF), after an overnight period of serum starvation. Despite finding a few differences in constitutive expressions and levels of activation of ERK 1/2 between DU-145 and PC-3 cells, we concluded that FucSulf1 did not abrogate any detectable growth factor stimulation.

FucSulf 1 decreases tumor cell spreading: A possible role for neuropilin-1 and focal adhesion kinase

Given that matrix-dependent adhesion, along with mitogenic growth factors, also dictates progression from G1 through S phases during the cell cycle (Schwartz and Assoian 2001), we decided to inspect more closely the effect of FucSulf1 on cell spreading and morphology. When prostate cancer cells were incubated with FucSulf1 for 48 h, remarkable changes in cell spreading were observed with DU-145 cells (Fig. 2A–C) and PC-3 cells (Fig. 2D–F). For both cell lines, actin cytoskeleton significantly shifted from a prevailing stress fiber organization to either a cortical localization, or to a punctuated cytoplasmatic distribution (details magnified on panels *b* and *e*), besides an evident decrease in cell spreading, as compared

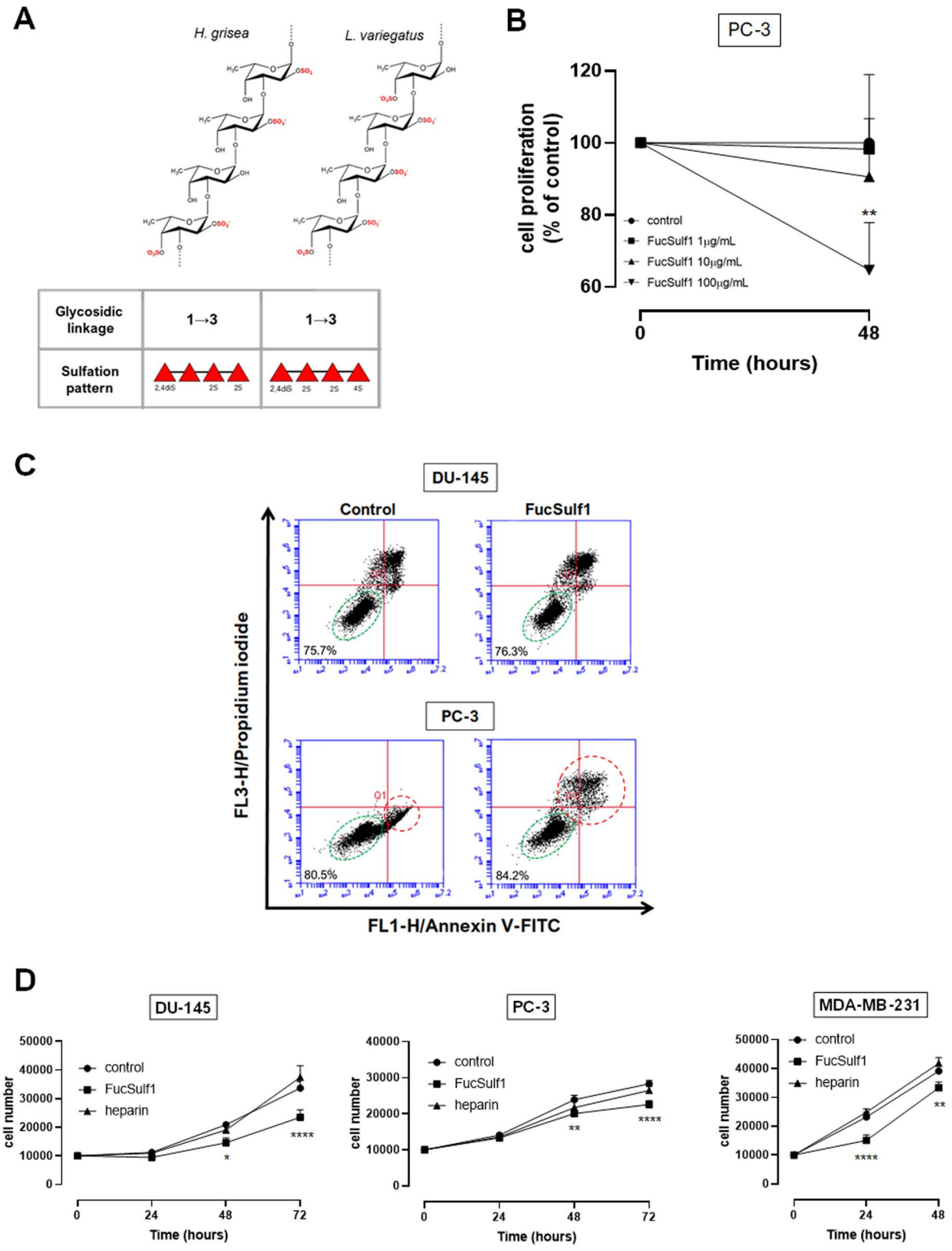

Fig. 1. Inhibition of tumor cell proliferation by sulfated fucans. (A) Sulfated fucans from marine echinoderms have a regular repetitive unit, which vary among different species. FucSulf1 (from *L. variegatus*) and FucSulf2 (from *H. grisea*) share the same [1 → 3] glycosidic bonding, while slightly differing in their pattern of sulfation at positions 2 (2S) and 4 (4S) of their fucose residues (represented as red triangles); α-L-fucose symbol follow the SNFG system (Varki et al. 2015). (B) PC-3 prostate cancer cells were incubated in the presence of the different concentrations of FucSulf1 (1, 10, and 100 μg/mL), and proliferation was measured at the endpoint of 48 h, as described in the Materials and Methods section. $^{**}P < 0.001$, $n = 5$; (C) DU-145 and PC-3 prostate cancer cells were analyzed for their viability parameters (apoptosis/necrosis profile) by flow cytometry, after incubation with 100 μg/mL FucSulf1 for 48 h. Images are from a representative experiment ($n = 4$); percentual numbers shown on the bottom left of each panel represent the mean for all 4 experiments. Cell populations exhibiting (^{low}annexinV/^{low}PI) labeling profiles, encircled by green dashed lines represent the viable subpopulation, whereas red dashed circles indicate cellular subpopulations prone to, or engaged into apoptosis/necrosis. (D) Time-course of cell proliferation of prostate cancer cells (DU-145, PC-3), and MDA-MB-231 breast cancer cells, in the presence of sulfated polysaccharides (FucSulf1 or heparin), both at 100 μg/mL, for 48 h. For the indicated comparisons, $^{*}P < 0.02$; $^{**}P < 0.001$; $^{****}P < 0.0001$ ($n = 4$).

with untreated cells (*a* and *d*) and to heparin-treated cells (*c* and *f*). Confocal analysis (Fig. 2G) allowed us to confirm the occurrence of loss of spreading in PC-3 cells treated with FucSulf1, a morphological shift that solidly correlates with measurable increments in nuclear height, a valuable parameter for assessing cell spreading (Li et al. 2015). Nuclear heights in cells treated with heparin did not significantly differ from the measures obtained for untreated control cells.

The dynamics of actin cytoskeleton at sites of cell adhesion to the matrix is closely regulated by focal adhesion kinase (FAK), a nonreceptor tyrosine kinase that acts as a primary regulator of cell adhesion signaling, to modulate cell proliferation, survival, and migration (Sulzmaier et al. 2014). We then decided to investigate whether the treatment of DU-145 and PC-3 cells with FucSulf1 modulated the activity of FAK.

As shown in Fig. 2H, FucSulf1 decreased the amount of phosphorylated FAK (tyrosine Y^{397} site) by ≈40% in DU-145 and ≈60% in PC-3 cells, suggesting that this sulfated fucan interfered with integrin-dependent cell adhesion. Overall decrease of total and activated FAK levels in FucSulf1-treated cells seemed to be related to FAK degradation, since a noticeable 90 KDa band, recognized by the anti-FAK antibody, appeared in this condition, for both cell lines (Fig. 2H). It is worth noting that, in some experiments, the fraction of phosphorylated FAK could not be estimated, as the FAK band nearly disappeared from the lysates (Fig. S2A). We also observed that the levels of neuropilin-1 (NRP-1), a multifunctional membrane co-receptor implicated in FAK activation (Zeng et al. 2014) and involved in enhancement of cell responses to several growth factors and extracellular ligands (Guo and Vander Kooi 2015) were also decreased after 48 h of incubation of both prostate cell lines—and specially of PC-3 cells—with FucSulf1. In contrast, heparin treatment of DU-145 and PC-3 cells was not able to decrease FAK activation, or to significantly modify NRP-1 and FAK levels in cell extracts (Fig. 2H).

Endocytosis of NRP-1 and β1 integrin was increased in prostate tumor cells treated with FucSulf1

The adhesive matrix glycoprotein fibronectin (FN) is functionally related to integrins and neuropilins, since FN fibril assembly in matrices was shown to be dependent on $\alpha5\beta1$ integrin and NRP-1, in both in normal and transformed cells (Valdembri et al. 2009; Yaqoob et al. 2012). The relaxation of cell adhesion caused by integrin cluster destabilization or by full detachment of integrins from their ligands can promote receptor endocytosis (de Franceschi et al. 2015). After confirming that the cells used in the present work incorporated expressive amounts of FN in their matrices (Table S1), we then speculated that, if FucSulf1 could interfere with $\alpha5\beta1$/NRP-1-dependent adhesion, the triggering of endocytosis of these receptors would be an expected outcome. Therefore, we decided to investigate the endocytosis of both receptors ($\alpha5\beta1$ and NRP-1), with focus on PC-3 cell line, which was shown to express higher levels of NRP-1 protein (Fig. 2H, control).

Endocytosis of NRP-1, $\alpha5$-, and $\beta1$-integrin chains, as assessed by co-localization analysis of each receptor with EEA1 protein (a primary endosome marker), showed that the treatment of PC-3 cells with FucSulf1, but not with heparin, led to a significant increase in both NRP-1 (Fig. 3A) and $\beta1$-integrin internalization (Fig. 3B). Heparin treatment clearly decreased the presence of $\alpha5$-integrin in primary endosomes, as compared with both the control and the FucSulf1-treated condition (Fig. 3C). However, we did not observe statistically significant differences for $\alpha5$ chain endocytosis upon treatment with FucSulf1, as compared with untreated control (Fig. 3C).

Since FucSulf1 would be expected to also promote significant $\alpha5$-integrin chain internalization, as it did for its partner $\beta1$ chain, we directed our attention toward the specific reactivities of the antibodies used in the confocal analysis. Unlike the anti-$\beta1$ antibody, which recognized a cytoplasmic motif inside this integrin chain, the anti-$\alpha5$ monoclonal antibody used here was generated against an epitope located on the ectodomain of this integrin chain. Therefore, we also analyzed the presence of soluble forms of $\alpha5$ integrin and NRP-1 in the conditioned media of PC-3 cells, in the same conditions. In FucSulf1-treated cultures, we found an important number of fragments of both $\alpha5$-integrin (showing 50% of fragments heavier than 77 KDa) and NRP-1 (50% of fragments > 91 KDa), which were not observed upon heparin treatment, or in the control condition (Fig. S2B).

The attachment (or primary adhesion) of PC-3 cells to FN was not inhibited by pretreatment with FucSulf1, though a slight inhibition was observed with DU-145 cells (Fig. S3). In these experiments, we also included the analysis of another cell line relevant to the present study, the MV3 melanoma. As for the prostate cancer cell lines, FucSulf1 also decreased the relative amount of total and active FAK in MV3 cells (not shown). Taken together, these observations suggested that disturbances of cell spreading on FN-containing matrices, induced by FucSulf1, were probably a sufficient condition enabling the inhibitory activity of this sulfated fucan on tumor cell proliferation, through mechanisms that appear to be independent of primary attachment, and possibly related to the impairment of tumor cell spreading and to a decrease in FAK activity.

FucSulf1 and FucSulf2: 2 structurally related sulfated fucans with similar biological properties

The purification of FucSulf1 can be limited by seasonal availability of the sea urchin *L. variegatus*, besides a relative low yield of the procedure, which could eventually restrain FucSulf1 usage in preclinical studies. On the other hand, the sulfated fucan FucSulf2 (Fig. 1A) exhibits great structural and functional similarity with FucSulf1 and can be purified with high yield from the sea cucumber *H. grisea*. Both sulfated fucans, with discrete differences between them, have been considered as mild anticoagulant glycans, as compared with the powerful activity of UFH (Pereira et al. 1999). As shown in Fig. 4, FucSulf2, like FucSulf1, also induced loss of cell spreading, as demonstrated by the significant increase in cell nuclei heights (Fig. 4A), and decreased stress fibers, with a concomitant actin labeling in a dotted pattern (Fig. 4B, color details). Reinforcing their functional resemblance, FN was able to strongly bind to both immobilized sulfated fucans, in a concentration-dependent manner (Fig. 4C), suggesting that FucSulf1 and FucSulf2 could exert their biological effects by interfering with the organization of FN matrix.

Considering the perspective of exploring the role of sulfated fucans in vivo, we then decided to compare the effects of FucSulf1 and FucSulf2 using melanoma cell lines. Both sulfated fucans exerted effects on melanoma cell proliferation, by inhibiting ~45% in human MV3 cells, and up to 56% in mouse B16-F10 cells after 48 h of incubation (Fig. S4). The inhibition rate observed with the B16-F10 cell line was

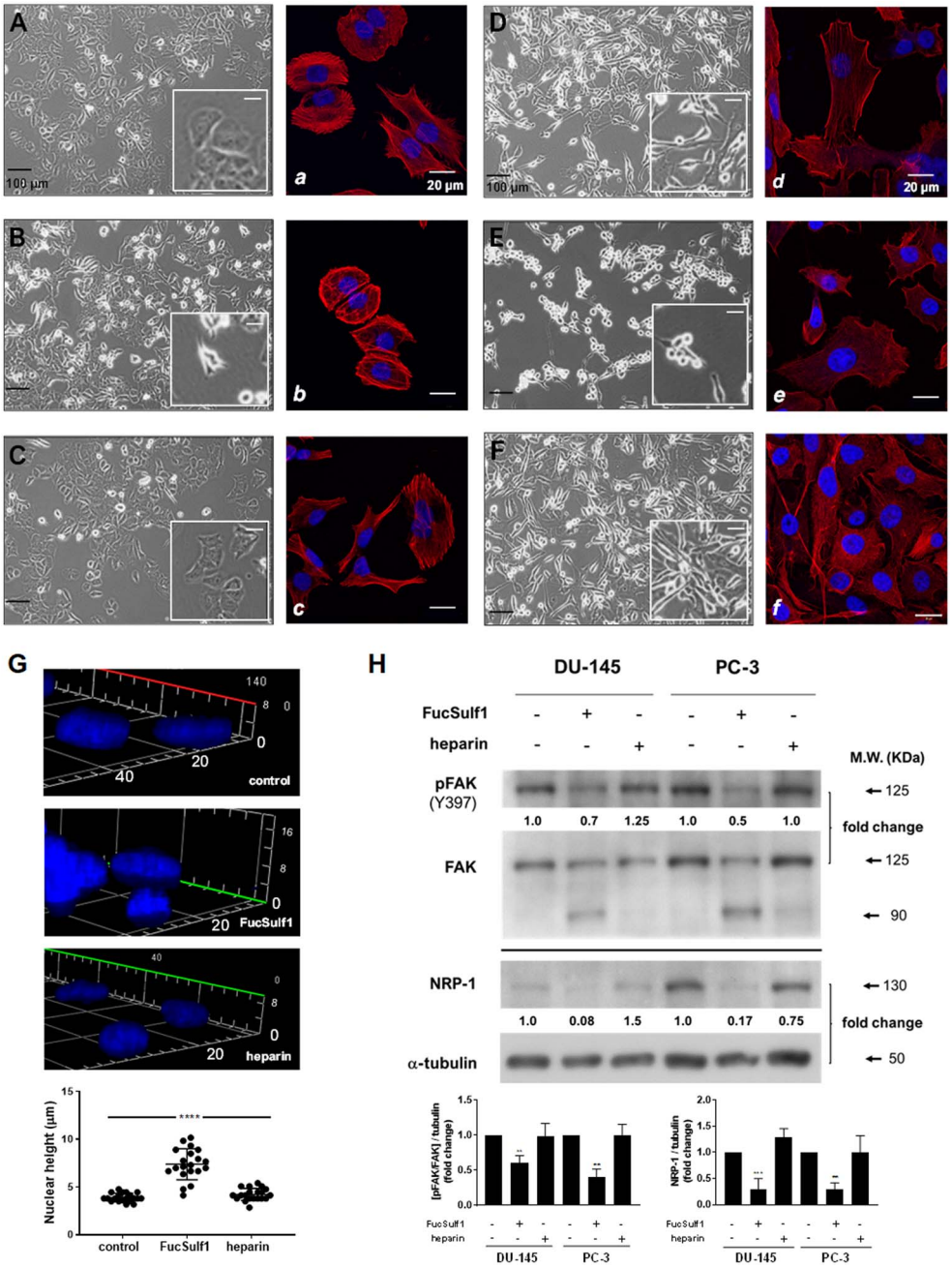

Fig. 2. Effect of FucSulf1 and heparin on tumor cell spreading and adhesion-dependent signaling. DU-145 cells A-C; *a–c*) and PC-3 cells D-F; *d–f*) were grown onto glass coverslips, for 48 h in absence A, *a*; D, *d*) or presence of FucSulf1 B, *b*; E, *e*), or heparin C, *c*; F, *f*) (both polysaccharides at 100 μg/ml), in medium containing 5% FCS. For immunofluorescence staining, cells were fixed and processed as described in Materials and Methods section, prior to co-incubation with nuclear staining reagent DAPI and rhodamine-phalloidin conjugate for visualization of polymerized actin. Images were captured using a bright field inverted microscope A-F), or with ×63 objective of a Zeiss LSM 510 meta confocal microscope *a–f*). Images represent a typical analysis, out of 3 experiments with comparable results. White scale bars = 20 μm, black scale bars = 100 μm; (G) estimation of cell spreading by quantification of nuclear height: PC-3 cells were treated with polysaccharides for 48 h and processed for confocal analysis (details in the Materials and Methods section). An angled 3D volumetric view was generated, with emphasis on DAPI staining (blue), followed by nuclei heights determination (white numbers scale expressed in μm). Measures were assessed in 3 different fields/condition (n = 20) using ZEN 2012 (black edition) software. **** $P < 0.0001$, for the indicated comparisons; (H) after growing prostate tumor cells for 24 h, cells were starved overnight and then incubated with FucSulf1 or heparin (both at 100 μg/ml) for 48 h. Cell monolayers were then lysed with RIPA buffer containing protease and phosphatase inhibitors. Western blots from whole-cells lysates were analyzed for total FAK, phospho-FAK ($pFAK^{Y397}$ autophosphorylation site), and NRP-1. Fold changes represent (pFAK/FAK) and [NRP-1/tubulin] ratios obtained from the pixel quantification of protein bands as compared with untreated controls (scored as 1.0), as described in the Materials and Methods section. Proteins in samples were separated using 10% acrylamide running gels in reducing conditions. Blot images represent a typical experiment (including its densitometric fold-changes in protein ratios, as indicated), whereas bar graphs represent the mean densitometric values obtained from at least 3 independent experiments for each set (FAK or NRP-1 analysis). In several experiments, nearly extinction of protein bands when treating cells with the sulfated fucan, precluded higher sample sizes for this quantitative estimation (see Fig.S2, for an example). Predicted molecular weights: FAK: 125 kDa; NRP-1: 130 kDa; α-tubulin: 50 kDa (loading control). ** $P < 0.002$, *** $P < 0.01$, as compared with both untreated and heparin-treated conditions, as indicated.

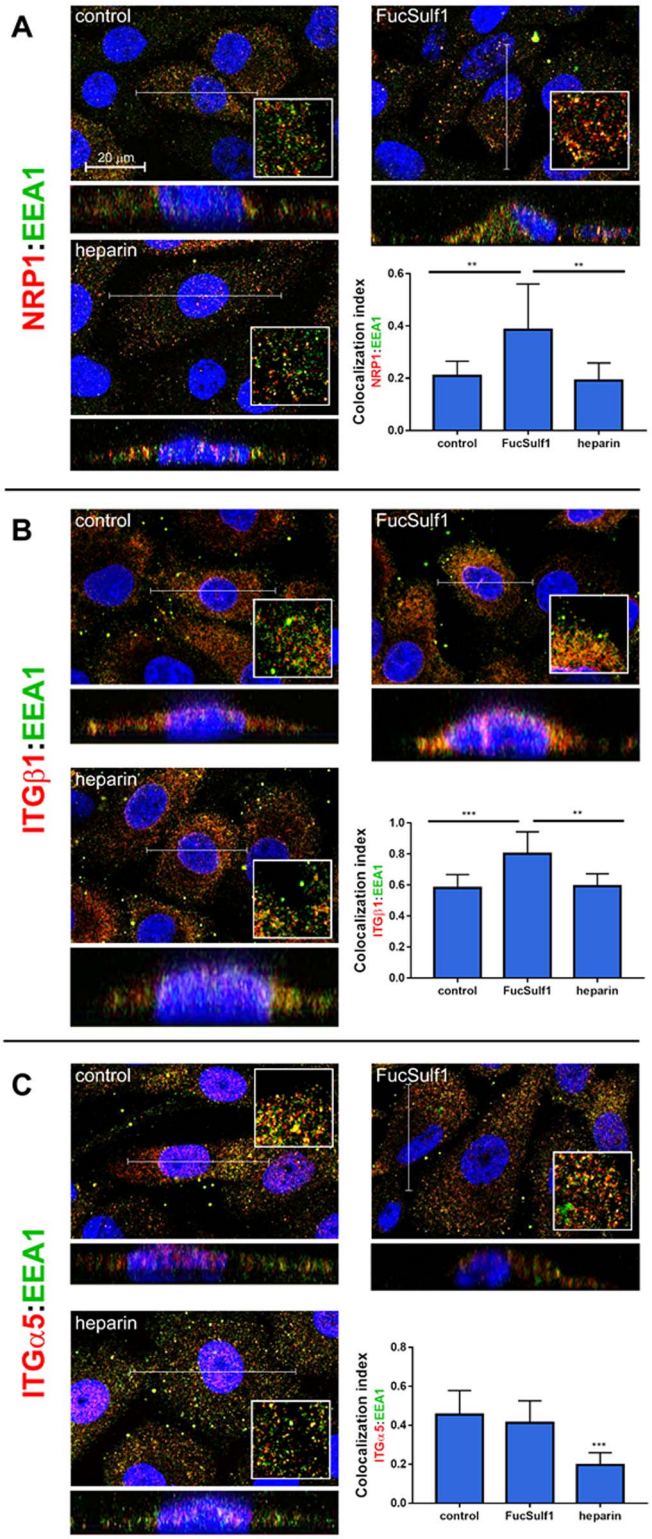

Fig. 3. Stimulation of NRP-1 and β1-integrin endocytosis by FucSulf1 treatment of PC-3 prostate cancer cells. PC-3 cells seeded on glass coverslips were treated with FucSulf1 or heparin (both at 100 μg/mL) for 48 h. Cells were fixed, permeabilized, and stained for fluorescence analysis, as described (details in the Materials and Methods section). Double staining was performed with a primary antibody against the endosomal protein EEA1 (detected with a secondary antibody conjugated with *AlexaFluor 488,* green) or each of the following proteins: (A) NRP-1, (B) β1-integrin, and (C) α5-integrin chains, all detected with an *AlexaFluor* 555 conjugate, in red. Nuclei were stained with DAPI (blue). Slides were analyzed under a LSM 510 META (Zeiss) inverted confocal microscope ($\times$63 magnification) and image acquisition (Z-stacking) was performed using the ZEN 2012 (black edition) software. For each image inside panels A, B, or C, an orthogonal projection was provided for a representative cell (projection axis represented by the white lines), together with detailed inserts highlighting the overlapping pixels (a 2-fold digital magnification of cytosolic regions from the same representative cell). On the bottom right of each panel, graphic bars represent the quantification of co-localized events, calculated from the analysis of 20 ROIs (1 ROI/cell), selected from at least 3 deconvoluted fields per condition (each field = equidistant confocal slice with thickness of 0.8 μm). MCC for each ROI, provided by the Coloc2 plugin of *Fiji-like ImageJ* software, were used to perform statistical comparisons; $^{**}P < 0.006$; $^{***}P < 0.0006$, for the indicated comparisons.

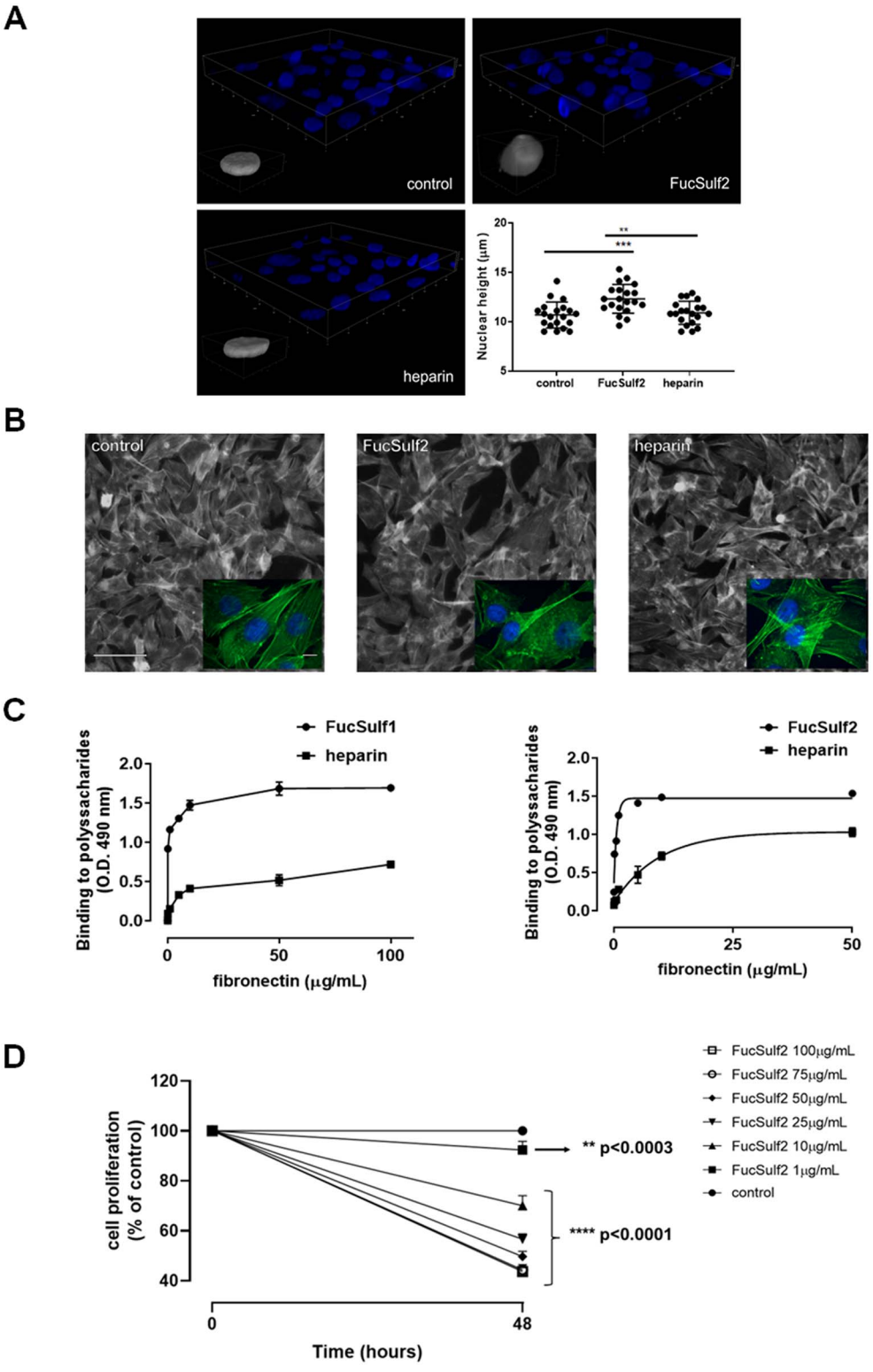

Fig. 4. FucSulf1 and FucSulf2, 2 structurally related sulfated fucans with similar effects on cell spreading and proliferation. (A) Human MV3 melanoma cells were seeded on glass coverslips, treated for 48 h with FucSulf2 or heparin (100 μg/mL), then fixed and processed for fluorescence analysis, as described in the Materials and Methods section. The heights of DAPI-stained nuclei (in blue) were measured in reconstructed 3D images by confocal microscopy; calibration grids on images are expressed in micrometers (μm); $^{**}P < 0.003$, $^{***}P < 0.001$. (B) Organization of microfilaments analyzed by fluorescence microscopy of the same MV3 cells pictured in a), following cellular staining with AlexaFluor 488-phalloidin (green fluorescence). (C) Concentration-dependent binding of FN to immobilized FucSulf1, FucSulf2, and heparin: soluble FN (0.05–100 μg/mL) was incubated with polystyrene wells previously coated with polysaccharides (100 μg/mL), and binding was detected by indirect ELISA. (D) Mouse B16-F10 melanoma cells were incubated in the presence of FucSulf2 (growing concentrations in the range 1–100 μg/mL), and proliferation was measured at the endpoint of 48 h, as described in the Materials and Methods section; the exhibited *P*-values refer to comparisons with the control (untreated) condition. Panels in a, b) are representative images of assays repeated 5 times.

almost double the rate observed for prostate cells (~30% of inhibition), when using FucSulf1 at 100 μg/mL (Fig. 1D). FucSulf2 also decreased the FAK and NRP-1 levels in MV3 cells (not shown). Using a concentration range of FucSulf2 between 1 and 100 μg/mL, we observed that concentrations as low as 1 μg/mL inhibited about 10% of B16-F10 cells proliferation, whereas with 10 μg/mL, a 30% rate of inhibition was achieved (Fig. 4D), suggesting that the inhibitory effect of FucSulf2 is at least 10 times more potent in melanoma cells than in prostate carcinoma cells.

Since FAK activity has been characterized as a major regulator of cell migration and invasion in embryonic, adult, and tumor tissues (Zhao and Guan 2011), we tested the effect of FucSulf1 on the migration of B16-F10 murine melanoma cells, using the wound healing assay, as this cell line was our model of choice for in vivo assays (Fig. 5A). FucSulf1 inhibited the monolayer wound closure by ~65% after 72 h, whereas heparin treatment appeared to accelerate cell migration up to 48 h of treatment, when compared with the untreated condition. After 72 h, the heparin and control conditions resulted in similar outcomes, with the closure of ~90% of the scratching lesion. Then, using FucSulf2, we verified if it could inhibit the invasion of a basal lamina matrix (Matrigel, polymerized on the upper compartment of 8 μm pore inserts) by human melanoma MV3 cells (Fig. 5B). We found that FucSulf2 was able to inhibit matrix invasion by ~30%, compared with the untreated control. Heparin had no effect in this assay. These results demonstrated that both sulfated fucans were able to interfere with cellular skills that crucially rely on FN-mediated FAK activation.

To further compare the effect of both sulfated fucans across the cell lines selected for this investigation, we decided to also challenge the PC-3 prostate cancer cells with FucSulf2, given that, in the present work, essential data were obtained by treating this cell line with FucSulf1 (Fig. 1–Fig. 3). Reinforcing their structural and functional similarity, FucSulf2 also exhibited critical effects on PC-3 cell migration, inhibiting by 51% after 48 h and 35% by 72 h (Fig. 5C), whereas heparin again seemed to accelerate the process, and promoted a full wound closure by 48 h of assay. Furthermore, when PC-3 cells were incubated with FucSulf2 for short periods of time at 4°C and then analyzed by flow cytometry, we found significant decreases in the expression of the integrin $\alpha 5$-chain on the surface of these cells, of ~19 and ~28%, after 30 and 60 min of treatment, respectively (Fig. S5). Taken together, these results corroborated evidence for a functional similarity between FucSulf1 and FucSulf2 and toward different cancer cell types.

FucSulf1 and FucSulf2 inhibit tumor growth in vivo: modulation of FAK

We then decided to investigate the effect of FucSulf1 and FucSulf2 on tumor growth in vivo, using a well-established experimental model of subcutaneously implanted tumor in mice (Khanna and Hunter 2005). The size of tumors was determined every 2 days. FucSulf1 delayed tumor growth, whereas heparin effect was indistinguishable from the one observed in PBS-treated animals (Fig. 6A). Noteworthy was that both control and heparin-treated mice presented illness symptoms and were more apathetic from day 15 onwards, since tumor inoculation. Two of control animals died on day 20, whereas mice treated with FucSulf1 seemed healthier than the untreated group or the heparin-treated group, with no signs of illness throughout the testing period (20 days).

We also conducted experiments to investigate possible antitumor effects of FucSulf2 in vivo. Tumors were surgically removed after 15 days of the experiment. We found that treatment with FucSulf2 slowed the growth of tumors from the 7th day of treatment (Fig. 6B), which resulted in noticeably smaller tumors at the end of the experiment (Fig. 6C, image panel), confirmed by the lower weight (Fig. 6D) than those observed in mice treated with placebo (buffered saline) or with heparin, by the end of the trial. Noteworthy was that most of the animals treated with FucSulf2 showed normal motor activity and defense reflexes, healthy fur, and normal weight. Two specimens from the FucSulf2 treatment group did not develop any palpable tumors, nor did bear any tumor mass that could be found upon surgery (symbolized by ∅ in Fig. 6C), an event that was not observed in any animals of the other 2 experimental groups (untreated controls and heparin-treated animals).

Tumors in heparin-treated mice and in untreated animals exhibited similar patterns, suggesting that heparin, unlike FucSulf2, did not show antitumor activity at primary implantation sites, in this animal model. Indeed, in both the control and heparin treatment conditions, the animals were apathetic at the end of the trial. In the control condition, one specimen died (tagged with the symbol †).

We also analyzed FAK signaling in tissue extracts prepared from tumors isolated from the in vivo experiments represented in Fig. 6C. When analyzing total FAK, we noticed that the 90 kDa degradation band could be observed in all conditions, but more intensely in tumors from animals treated with FucSulf2. We also observed a decrease in $pFAK^{Y397}$ in samples from animals treated with FucSulf2, and immunoprecipitated bands were mostly detectable in the molecular weight region between 80 and 95 kDa, which may correspond to less active, or even inactive forms of FAK (Fig. 6E). In the control (animals treated with PBS) and in the heparin treatment condition, even though fragmentation was also apparent, pFAK with the expected molecular weight (125 kDa) was detectable in these conditions (Fig. 6E). This set of results suggested that FucSulf2 is capable of interfering with the same adhesion receptors and signaling pathways already identified as targets for FucSulf1, strengthening the functional similarities between these 2 sulfated fucans.

Discussion

In the present study, we evaluated the antitumor effects of two sulfated fucans: FucSul1 and FucSulf2, extracted from the echinoderms *L. variegatus* and *H. grisea* (Fig. 1A), respectively, as an attempt to prospect pharmacologic alternatives to the use of heparin, for which harmful side effects have been described in cancer therapeutics. Both molecules exhibit regular sequences having in common a 2,4-disulfated fucose unit, and it has been postulated that 2-O- or 2,4-di-O-sulfations are mostly anticoagulant motifs in the structure of these sulfated fucans (Pomin and Mourão 2014). Whether these structural motifs may also contribute for their antitumor activity, as described in the present work, still remains an unsolved question that we intend to address in the future. In addition to the structural similarity, FucSulf2 presents a much higher

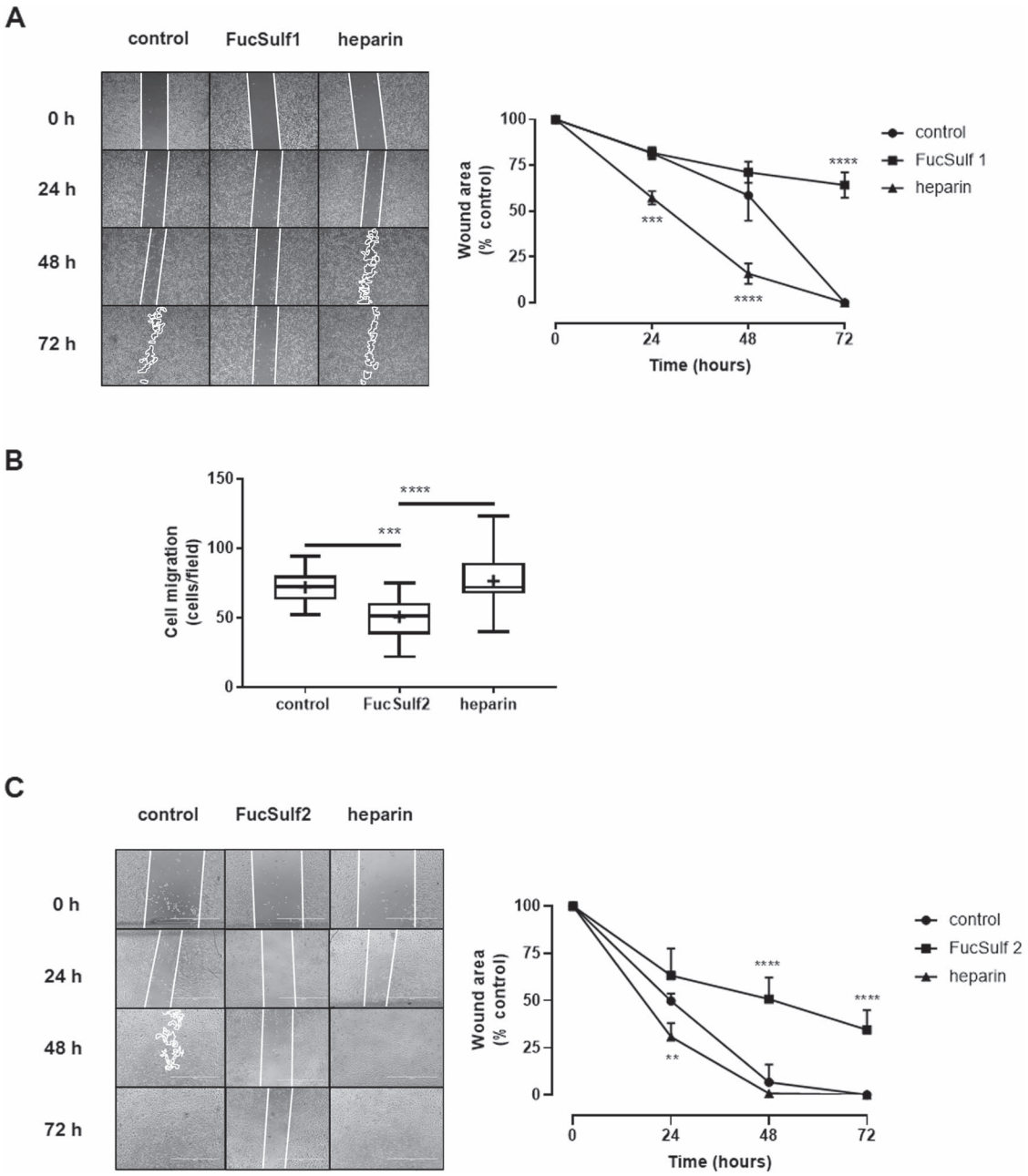

Fig. 5. FucSulf1 and FucSulf2 inhibit FAK-dependent motile properties in melanoma cells. (A) Confluent monolayers of murine B16-F10 cells were pretreated with mitomycin-c, before being lesioned with a plastic tip. Lesion closure was quantified at 24, 48, and 72 h, in the presence of FucSulf1 or heparin (100 μg/mL), using the *image J* software; ***P = 0.0004; ****P < 0.0001; n = 5; (B) MV3 cells were allowed to migrate for 18 h through a Matrigel layer poured into 8 μm porous inserts. Transmigrating cells were labeled on the lower side of the insert with DAPI and counted in 10 fields/condition, in an inverted fluorescence microscope; ***P < 0.0002; ****P < 0.0001; n = 5; (C) confluent monolayers of human PC-3 prostate cancer cells were pretreated with mitomycin c), before being lesioned with a plastic tip. Lesion closure was quantified at 24, 48, and 72 h, in the presence of FucSulf2 or heparin (100 μg/mL), using the *image J* software; **P = 0.02; ****P < 0.0001; n = 3.

yield in its purification than FucSulf1, an aspect that could become relevant when considering their further preclinical, or even possible clinical applications.

A recent study, based on a combination of nuclear magnetic resonance (NMR) spectroscopy and molecular dynamics analysis of the conformation and dynamic of sulfated fucans, showed that sulfation patterns can give rise to either dynamic or rigid portions inside sulfated fucans chains (Queiroz et al. 2015). In the case of FucSulf1, the flexibility occurs at glycosidic linkages flanking rigid tetrasaccharide-repeating units. The rigid structures were considered likely to interact far more effectively with coagulation cofactors. Indeed, these structural studies would rather corroborate the idea that inhibitory biological effects of sulfated fucans were not necessarily related to negative charge density per se, since heparin, which is preponderantly composed of disulfated α-glucosamine units (N- and 6-sulfation), showed no inhibitory action in the functional cell assays performed with different tumor cell lines in the present work.

We started our studies on possible direct antitumoral effects of the sulfated fucan isolated from *L. variegatus*, using two cell lines originating from prostate adenocarcinomas, namely,

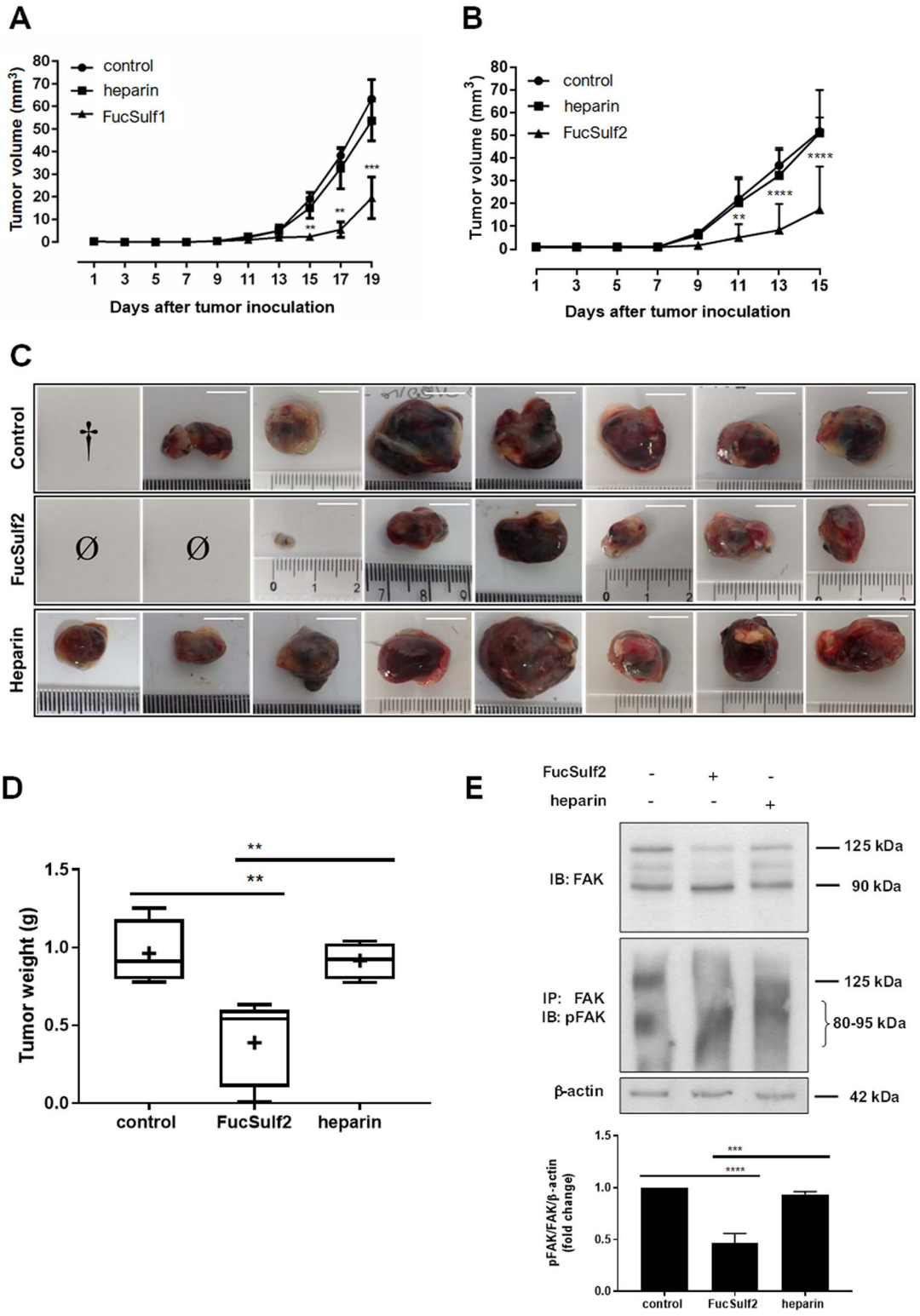

Fig. 6. FucSulf1 and FucSulf2 inhibit tumor growth in vivo. (A) and (B) B16-F10 murine melanoma cells in serum-free RPMI medium were inoculated (2×10^5 cells/animal) into the right flank of C57/BL6 mice, on day 0. From the day after inoculation (day 1), the mice began to receive daily intraperitoneally FucSulf1 (A), FucSulf2 (B), or heparin (A, B), whereas the control animals received sterile PBS. From day 2 of treatment, tumor volumes were checked with a caliper every 2 days, until the end of the test, and tumor volumes were calculated; $^{**}P = 0.003$; $^{***}P < 0.002$; $^{****}P < 0.0001$; $n = 8$; (C) morphological aspect of the experimental tumors: at the end of 15–20 days of treatment (see text for details on endpoints, for each sulfated fucan protocol) with PBS (control) or polysaccharides, animals were anesthetized and sacrificed, the tumors removed, measured, and photographed; † = specimen death; Ø = no tumors found; (D) the tumors (from 8 animals per group) excised and shown in (C) were also weighed; $^{**}P = 0.005$ (FucSulf2 versus control), $^{**}P = 0.009$ (FucSulf2 versus heparin); (E) tumors from animals treated with FucSulf2 exhibited increased FAK degradation, with decreased kinase phosphorylation: protein extracts (20 μg/lane in 10% resolving PAGE-SDS gels), prepared from tumors from animals under different treatments (PBS-control, FucSulf2, and heparin) were analyzed by either direct western blotting (total FAK, upper panel), or by WB after immunoprecipitation (enrichment for detection of phosphorylated forms; middle panel). Blot images represent a typical experiment (including its densitometric fold-changes in protein ratios, as indicated), whereas bar graphs represent the mean densitometric values obtained from at least 3 independent experiments for each set. $^{***}P = 0.0001$, $^{****}P < 0.0001$.

DU-145 and PC-3 cells. FucSulf1 was able to significantly inhibit the proliferation of both prostate cancer cells. Even though the PC-3, unlike DU-145 cell line, seemed to contain a subpopulation of apoptosis-primed cells that could resume the process under FucSulf1 treatment, we were not able to distinguish major impacts on the ratio of viable cells—i.e. cells exhibiting ^{low}annexinV/^{low}PI labeling profiles—that could possibly explain the significant decrease in cell proliferation caused by the treatment with FucSulf1. Also, both FucSulf1 and FucSulf2 were near twice as effective in inhibiting the proliferation of melanoma cells (from human and murine sources), as compared with prostate cancer cells.

In our hands, the activation status of the central signaling pathways controlling cell proliferation and survival, such as MAPKs and Akt/PKB, was not impacted by FucSulf1, even when pro-growth stimuli were provided, by challenging prostate tumor cells with EFG and FGF-2—2 important effectors of tyrosine kinase receptors in cancer (Regad 2015). Although tumor cells can express VEGF receptors (Goel and Mercurio 2013), the cell lines in our study were not able to respond to VEGF with increasing proliferation or ERK activation (our unpublished results).

Besides growth factor-dependent signaling, cell-matrix adhesion is also critical for the survival and proliferation of cells. It converts mechano-sensing processes into chemical cell signaling, mainly through members of the superfamily of integrin receptors (Hytönen and Wehrle-Haller 2015). We found that the treatment of prostate tumor cells with FucSulf1 lead to a significant loss of cell spreading. Interestingly, we observed that the autophosphorylation of FAK-Y^{397} site was importantly decreased in these cells, an event that seemed related to the reduction of the total amount of FAK protein in FucSulf1-treated cells. Inhibition of this critical adhesion-dependent kinase, or a possible shift in its turnover (as we may further discuss ahead in this text) could account for the effect of FucSulf1 as an inhibitor of tumor cell proliferation, since FAK activation and overexpression promote tumor growth (Sulzmaier et al. 2014).

Additionally, the 130 kDa chain of NRP-1 was barely detectable by western blotting, after the long-term treatment (48 h) of prostate cancer cells with FucSulf1. Interestingly, neuropilins (NRP-1 and NRP-2), which are type I transmembrane proteins well conserved in all vertebrates, have been positively associated to poor prognosis of neoplasia, for prostate and melanoma cancers (Chaudhary et al. 2014; Graziani and Lacal 2015). NRP-1, originally reported for its role in cell adhesion and guidance, is now considered as an adhesion co-receptor for integrins. In the context of the present study, it is relevant to note that NRP-1 promotes $\alpha5\beta1$-dependent FN matrix assembly in tumor microenvironment, an event that strongly stimulates tumor growth (Yaqoob et al. 2012). Work done by others also stressed the important role of NRP-1 in FAK activation in pancreatic, glioma, and breast cancer cells (Fukasawa et al. 2007; Chen et al. 2014; Zeng et al. 2014). Thus, the hypothesis that FucSulf1 could disturb functional connections between NRP-1 and FN-dependent integrins clearly emerged from our observations.

The role of FN in tumor progression has been the subject of debate for over 4 decades. While a tumor suppressor activity for cell surface-associated FN has been described in a few seminal observations (Hynes et al. 1979), FN organized into fibrils in the ECM microenvironment has been associated with increased malignancy, invasiveness, and poor prognosis of tumors (Spada et al. 2021). Indeed, the architecture of FN assembly in the ECM, also known as fibrillogenesis, was previously shown to sustain both FAK activation and cell cycle progression through G0/G1 → S phase checkpoint (Sechler and Schwarzbauer 1998; Sottile et al. 1998). The interaction of FN with cell surface HSPGs, and especially with syndecan-4, was shown to be crucial for the maturation of focal adhesions and promotion of full spread phenotype, in cooperation with integrins (Woods et al. 2000). Recently, it was demonstrated that HSPG is also necessary for the early formation of nascent FN/collagen I fibrils at matrix assembly sites (Hill et al. 2022).

In the present work, we could demonstrate that FN was able to efficiently bind to immobilized FucSulf1, FucSulf2, and heparin in vitro. FucSulf1 and FucSulf2 led tumor cells to adopt a round, poorly spread phenotype, whereas heparin—as expected from the literature on focal adhesions (Woods et al. 2000), favored primary adhesion and supported cell spreading instead. The possibility that these sulfated fucans could hinder FN interactions with syndecan-4, thus leading to cell rounding, deserves further investigation.

On the other hand, a pro-tumoral role of fibrillary FN in tumor matrices is also consistent with the fact that this glycoprotein is considered a major marker of accomplished epithelial-mesenchymal transition (EMT), a process that enhances motile behavior and oftentimes gives rise to invasive tumor cells (Kalluri and Weinberg 2009). Inhibition of FN fibrillogenesis blocks the activation of the transforming growth factor-β signaling pathway, which is a cytokine that crucially drives EMT progression (Griggs et al. 2017). Interestingly, we found that both FucSul1 and FucSulf2 were able to significantly inhibit prostate cancer and melanoma cell migration, evidence that is in accordance with the decrease in FAK activity observed in our experiments with both prostate and melanoma cancer cells. Thus, it also seems important to investigate whether the treatment of tumor cells with FucSul1 and FucSulf2 could lead to disturbances in the cell-dependent FN fibrillogenesis process, as well as in FN fibrils turnover.

Some integrins, including $\alpha5\beta1$, $\alpha6\beta4$, $\alpha M\beta2$ and $\alpha IIb\beta3$, are continuously internalized from the cell surface and subsequently recycled (Sczekan and Juliano 1990), a process intimately coupled to FN matrix remodeling itself (LaFlamme et al. 2008). NRP-1 was found to co-participate, in endothelial cells, in the regulation of endocytic trafficking of $\alpha5\beta1$ integrin (Valdembri et al. 2009). We found that FucSulf1 also promoted NRP-1 and $\beta1$-integrin endocytosis in PC-3 cells, with significant accumulation of both receptors in cell endosomes. This is consistent with the evidence that the relaxation of integrin clustering or its detachment can favor receptor endocytosis (de Franceschi et al. 2015).

We were initially intrigued by the lack of positive correlation between the internalization of $\alpha5$ integrin and its companion $\beta1$ chain—which together form the most relevant FN receptor. Regardless the fact that this observation was linked to the choice of an anti-$\alpha5$ chain antibody raised toward the extracellular domain of this integrin, this allowed us to identify receptor fragments in the conditioned medium collected from our assays, thus explaining the receptor underestimation inside cells. Effectively, we detected a myriad of degraded forms of $\alpha5$-chain and, to a lesser extent, of NRP-1, in the conditioned medium of cells treated with FucSulf1 after 48 h of treatment with FucSulf1, whereas only residual amounts of both receptors were detectable in the

media harvested from either untreated cultures or from cells treated with heparin. At this point, it has not been possible yet to distinguish the mechanism of generation of such fragments. It was shown that the loss of cell spreading, triggered by rarefaction of FN in matrices, induced pro-MMP-2 activation by MT-MMP, whereas integrin clustering and cell spreading inhibited the expression of MT-MMP (Yan et al. 2000). Two broad classes of proteases, MMPs and ADAMs, have been implicated so far in shedding of cell adhesion receptors (Miller et al. 2017). Given the significant effect of FucSulf1 and FucSulf2 in inhibiting cell spreading (e.g. by inducing cell rounding), MMPs as shedding effectors seem worthy of investigation.

The precise elucidation of integrin/NRP-1 endocytosis and recycling in cells treated with sulfated fucans seems necessary, not only to appropriately frame the fate of these receptors, but also to clear the possible effect of these polysaccharides on FAK turnover. We detected the increase of a 90 kDa FAK fragment in prostate cancer cells treated with FucSulf1. In vivo, using FucSulf2, a few bands were also detected in the molecular weight range between 80 and 95 kDa in tumor extracts, which may correspond to less active forms of FAK. In the control condition (animals inoculated with PBS) and in the heparin treatment condition, despite fragmentation was also apparent, the amount of pFAK with expected molecular weight (125 kDa) was higher when compared with the amount of pFAK in tumor extracts from animals treated with FucSulf2.

FAK cleavage products displaying similar molecular weights and generated by calpain-1 and calpain-2 have already been described by others, when investigating the focal adhesion turnover induced by degraded collagen fragments. FAK proteolysis by calpains and caspases has been implicated in the destabilization of focal adhesions, with broad implications for cell proliferation, migration, and apoptosis (Carragher et al. 1999). Interestingly, the pharmacologically targeted degradation of FAK, induced by a synthetic small molecule that directs this kinase to the ubiquitin proteasome system with high selectivity, was able to inhibit PC-3 cells migration and invasion much more efficiently than a small ATP-competitive FAK inhibitor presently being investigated in oncologic clinical trials (Cromm et al. 2018). This highlights the potential therapeutic interest of FucSulf1 and FucSulf2 as inducers of FAK degradation, both in vitro and in vivo. FAK and NRP-1 have been recently uncovered as targets, intensively scrutinized for the development of new anticancer drugs (Graziani and Lacal 2015), and may represent an exciting opportunity for fine-tuning pharmacologic inhibition of adhesion-dependent proliferation, especially in dual therapy: targeting cell adhesion-mediated resistance to both radiation and drugs has become a key strategy to sensitize aggressive cancers to these first-choice treatments (Dawson et al. 2021).

The antitumoral activity of these sulfated fucans seemed to be rather of cytostatic nature, as they neither inhibited major cell proliferation signal pathways, nor induced cell death in vitro. Although these outcomes would be expected from the ability of FucSulf1 and FucSulf2 to inhibit migration and invasion, observed in vitro, both being skills crucially dependent on FAK activity in aggressive malignant melanoma (Hess and Hendrix 2006), one may consider that the decreased melanoma growth rate in vivo could also partially reflect the interference, by the sulfated fucans, in other crucial cellular mechanisms, such as angiogenesis, a process that largely relies on heparin/HSPG-dependent factors (Xie and Li 2019). Figure 7 summarizes the findings of the present work and the gaps that still need to be addressed, regarding the antitumor mechanism of the sulfated fucans under investigation.

In conclusion, FucSulf1 and FucSulf2, two sulfated fucans with mild anticoagulant activity, isolated from echinoderms, arise from this study as candidates for the design of possible viable alternatives to the complications of long-term treatments of cancer patients with heparins, since they exhibited a potential for targeting tumor cells directly, by critically modulating key adhesion-dependent receptors and signaling pathways.

Materials and methods

Reagents

Unless otherwise stated, cell culture media and reagents were obtained from Thermo-Invitrogen/Life Sciences (São Paulo, Brazil). ECL Plus western blotting detection reagents and photographic film, and Pierce BCA Protein Assay Kit were from Thermo Fisher Scientific (São Paulo, Brazil); QuickStart Bradford Protein Assay was from Bio-Rad (Rio de Janeiro, Brazil). Protease and phosphatase inhibitor cocktails were from Merck/Sigma-Aldrich (São Paulo, Brazil). UFH (97/578, 229 IU mg^{-1}), that will be simply referred to as heparin, was obtained from the National Institute for Biological Standard and Control (UK).

Isolation and purification of sulfated polysaccharides

Sulfated fucans were extracted and purified as previously described (Mulloy et al. 1994; Ribeiro et al. 1994) either from the egg jelly coat of the sea urchin *L. variegatus* (FucSulf1), or from the body wall of the sea cucumber *H. grisea* (FucSulf2), whose structures are represented in (Fig. 1A), following the Symbol Nomenclature for Glycans (SNFG) system (Varki et al. 2015). The purity and structure of these sulfated fucans were checked by NMR spectra, as described (Castro et al. 2009).

Cell lines

Androgen-unresponsive human prostate cancer cell lines DU-145 (RRID: CVCL_0105) and PC-3 (RRID:CVCL_0105), mammary gland MDA-MB-231 adenocarcinoma cell line (RRID:CVCL_0062), and the mouse B16-F10 melanoma cell line (RRID:CVCL_0159) were originally obtained from American Type Culture Collection (ATCC). Human MV3 melanoma cell line (BCRJ Cat# 0284, RRID:CVCL_W280) has been previously characterized (van Muijen et al. 1991; Fonseca et al. 2010), originally provided by Dr Cezary Marcinkiewicz (Temple University, Philadelphia, PA), is now available from the BCRJ (Rio de Janeiro Cell Bank, Brazil). Cells were used between passages 15 and 30 and all cell lines were recently authenticated by the short tandem repeat (STR) fragment analysis, using the GlobalFiler PCR Amplification Kit (Thermo Sci., Waltham, MA, USA), by the DNA Diagnostic Laboratory, at UERJ (Rio de Janeiro, Brazil). The STR patterns found were equivalent to those available in the database provided by the ATCC (Manassas, VA, USA). MV3 cell line, which has not its STR profile deposited in

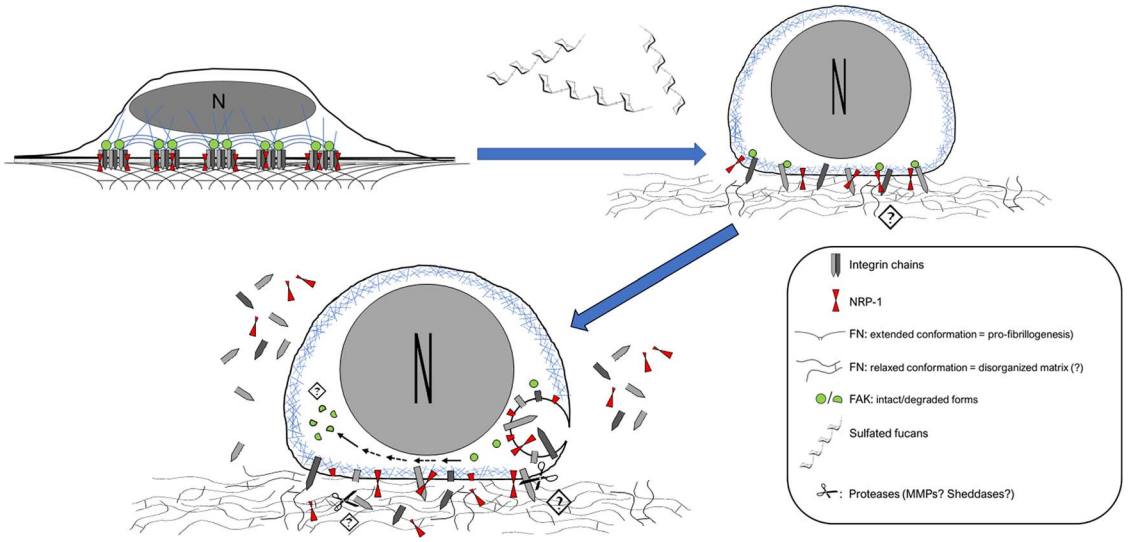

Fig. 7. A model for the effects of FucSulf1 and FucSulf2 on tumor cells. Treatment of tumor cells with the sulfated fucans triggers decreased cell spreading, possibly through increased turnover of integrin-dependent adhesion complexes and signaling machinery, crucial for cell proliferation and migration. While the steps marked with the symbol ? still deserve further investigation, we hypothesize that the interaction of sulfated fucans with FN fibrils disturbs matrix organization, possibly triggering the turnover of cell adhesion receptors ($\alpha5\beta1$ integrin, NRP-1, etc.) and FAK. Impairment of FAK-dependent signaling has major impacts on tumor proliferation, migration, and invasion.

public databases—was also analyzed (its profile can be made available for interested researchers, under request). Prostate and melanoma cells were maintained in RPMI 1640 medium, supplemented with antibiotics as above, 2 mM L-glutamine, and 10% fetal calf serum (FCS), at 37°C in a humidified 5% CO_2 atmosphere and harvested with 0.025% trypsin/0.02% EDTA or Accutase solutions from the culture flasks (Corning), according with experiments and cell types.

Cell viability assay

Tumor cells (1×10^5 cells/cm^2) were seeded in 6-well plates in RPMI 1640 medium containing 10% FCS, for 2 h at 37°C and 5% CO_2 atmosphere. Wells were then washed and incubated either with RPMI containing 5% FCS (control condition) or with polysaccharides (100 μg/mL, 150 μL/well) diluted in RPMI 1640 containing 5% FCS for 48 at 37°C, in 5% CO_2. Cells were detached with Accutase solution (Merck/Sigma) and the cell suspension was centrifuged for 10 min ($180 \times g$). Cell pellets were incubated with annexin and propidium iodide, following the instructions of the fabricant (*Annexin V: FITC* Apoptosis Detection Kit II/ BD Pharmingen). Stained cells were analyzed by flow cytometry (with a BD Accuri C6 Flow Cytometer).

Proliferation assay

Cells (1×10^4 cells/well or 5×10^4/cm^2, 200 μL/well) were seeded in 96-well plates in RPMI 1640 medium containing 10% FCS, for 2 h at 37°C and 5 % CO_2 atmosphere. The wells were then washed and incubated with RPMI containing 5% FCS (control condition) or with polysaccharides (in the range of 1–100 μg/mL, depending on the experiment; 150 μL/well) diluted in RPMI 1640 containing 5% FCS for 24, 48, and 72 h at 37°C, in 5% CO_2. A solution of 1 mg/mL MTT was incubated with wells at 37°C for 3 h at 5 % CO_2. The solution was then removed and replaced by 200 μL of isopropanol, and the absorbance was measured at 595 nm in a Victor NIVO microplate reader (Perkin Elmer, Waltham, MA, USA). The number of cells was deduced from a standard curve, obtained with tumor cells allowed to adhere on plastic for 2 h, which received the same treatment with MTT.

Western blotting analysis in cell cultures and tumor extracts

Cell signaling pathways and protein degradation were investigated in cultures (2×10^4 cells/cm^2) either grown in serum-supplemented media (for 30 min or 48 h) or under stimulation of growth factors, with or without FucSulf1 or heparin (both at 100 μg/ml). Details of these procedures are described elsewhere (*Supplementary Methods and Data File*). Cell extracts were prepared in ice bath with cold lysis buffer (1 μL/1,000 cells of 20 mM Tris, 150 mM NaCl, 1% Triton-X 100, containing 50 mM NaF, 1 mM Na_3VO_4), further supplemented with commercial protease and phosphatase inhibitors cocktails (Merck/Sigma-Aldrich, cat# P-8340 and P-5726, respectively). After cell layer scraping, lysates were aspirated and centrifuged at 16,800 $\times$ *g* for 20 min at 4°C. Total protein was determined before analyzing samples in 8 or 10% SDS-PAGE resolving gels (as indicated in figure captions), followed by protein transfer under gentle conditions (30 V/overnight at 4°C) to Immobilon-P PVDF membranes (Merck-Millipore Brazil, São Paulo). After saturation of membranes with 5% globulin-free BSA (Merck/Sigma-Aldrich, cat# A7030) in TBS-T (Tris buffered saline—50 mM Tris-Cl, pH 7.5, 150 mM NaCl, containing 0.1% Tween 20), they were incubated with the following set of primary antibodies (detailed in Table S2), all diluted in TBS-T containing 1% BSA: total and phosphorylated forms (between brackets) of AKT (AKT^{S473}), ERK (ERK$^{T202/Y204}$), FAK (FAK^{Y397}), and p38α (p38$\alpha^{Thr180/Tyr182}$), and the loading control proteins β-actin and α-tubulin. The cell receptors $\alpha5$ integrin chain and NRP-1 were analyzed in the conditioned media of cells in different conditions. Anti-mouse or rabbit secondary antibodies conjugated to horseradish peroxidase were used (Table S2). Protein bands were visualized using ECL detection system.

Films were scanned at high resolution (1200 dpi) and bands were quantified by using the dot measurement tools of the Adobe Photoshop software.

To analyze proteins in tumor samples by western blotting, tissue extracts were prepared through a combination of different mechanical and chemical procedures, all of them carried out at low temperature, namely: sequential freeze-thawing cycles, homogenization, ultrasonic bath incubation, and detergent lysis (10 mM HEPES, pH 7.4, containing150 mM NaCl, 1% IGEPAL CA-630, 0.1% SDS, 0.5% sodium deoxycholate, 20 mM NaF, and the protease/phosphatase inhibitors cocktails). The detailed procedure was described in the *Supplementary Methods and Data File*. After clarification of the lysates by centrifugation at 20,000 × *g* for 30 min at 4°C, total proteins in samples were quantified (by the BCA method) and lysates were aliquoted and kept at −80°C. For direct immunodetection of proteins in tumor extracts, 20 μg of total proteins/lane was analyzed in 10% SDS-PAGE resolving gels, before being transferred to PVDF membranes, as already described.

Detection of FN in tumor cell matrices by direct ELISA

Immobilized matrices secreted by confluent cells were obtained as described (Morandi et al. 1994). After a blocking step with 0.1% BSA/PBS-Ca^{2+} for at least 4 h at 37°C, wells were submitted to an indirect ELISA for FN detection in immobilized matrices, as previously described (Alves et al. 2011), using a rabbit polyclonal antibody raised against human FN (5 μg/mL) (Table S2), and a secondary antibody peroxidase conjugate (Table S2). A detailed version of the quantitative estimation of FN content is available elsewhere (*Supplementary Methods and Data File*). Revelation was performed with 1 mg/mL ortho-phenylenediamine in 0.1 M sodium citrate buffer, pH 4.5 (100 μl/well), and reaction was stopped with 1 M H_2SO_4 (50 μl/well). The microplate was read at 490 nm.

Solid-phase assays for assessment of the interaction of FN with sulfated polysaccharides

FucSulf1, FucSulf2, or heparin (100 μg/mL) was incubated in PBS with 96-well microplates, overnight at room temperature. After a blocking step with 0.1% BSA/PBS-Ca^{2+} for at least 4 h at 37°C, FN (0.05–100 μg/mL) in PBS-Ca^{2+} was added to the wells, overnight at 4°C. Incubations with primary and secondary antibodies, for detection of bound FN by ELISA, were performed as already described in Section 4.7. The microplate was read at 490 nm, as above.

Morphologic analysis of cell spreading and actin cytoskeleton organization

Tumor cells (DU-145, PC-3, and MV3), seeded either onto 6-well plates or 24-well plates (both at 2 × 10^4/cm^2) containing round glass coverslips (1.3 mm Ø), were allowed to grow in the absence or presence of sulfated fucans or heparin (100 μg/mL) for 48 h. Cells were fixed with 3.7% paraformaldehyde in PBS for 20 min at room temperature and then permeabilized with 0.1% Triton X-100 in TBS for 2 min. After a blocking step with 5% BSA, 10% donkey serum (Sigma-Aldrich, Cat# D9663) in TBS, the coverslips were incubated with rhodamine-phalloidin (0.1 μg/mL, Sigma) or AlexaFluor488-phalloidin (1:40, Molecular Probes/ThermoFisher Scientific, São Paulo Brazil) diluted in PBS containing 1% BSA. After staining, coverslips were mounted into the anti-fading reagent prolong with 4′,6-diamidino-2-phenylindole dihydrochloride (DAPI) (Molecular Probes/ThermoFisher Scientific, São Paulo Brazil). Images were captured using a digital EVOS-*fl* inverted fluorescence microscope (Thermo Scientific, São Paulo, Brazil), at the magnifications indicated in figures captions.

Quantitative analysis of endocytosis by laser confocal microscopy

Prostate cancer PC-3 cell line was seeded onto 24-well plates (both at 2 × 10^4/cm^2) containing round glass coverslips (1.3 mm Ø) and allowed to grow for at least 24 h. Cells were used at subconfluency in RPMI medium supplemented with 0.1% BSA. FucSulf1 or heparin (both at 100 μg/mL) was added for additional 48 h, and then cells on coverslips were fixed and permeabilized as described above. The primary antibodies and the dilutions used, always in TBS/5% BSA, are detailed in Table S2. Conjugates received additional 10% donkey serum (Sigma), to fade nonspecific staining. Coverslips were mounted into the anti-fading reagent prolong with DAPI. Slides were analyzed under a LSM 510 META Zeiss inverted confocal microscope, equipped with a 63 × P-Neofluar (NA 1.3), following excitation with the HeNe laser at 543 nm, and a 405 nm diode laser. Image Z-stacking acquisition and analysis were performed using the Zen 2012 software (Black Edition). Images were post-processed using the *Iterative Deconvolve 3D* plug-in from the open access NIH *Image J* software (https://imagej.net/Iterative_Deconvolve_3D, RRID:SCR_016246). Statistically significant co-localization was calculated from analysis of 30 regions of interest (ROI) (1 ROI/selected cell), collected from at least 3 different fields per condition (1 field = 1 equidistant confocal slice of 0.8 μm in thickness). Mander's co-localization coefficients (MCCs) were determined for each ROI using the *Coloc2* plugin of *Fiji (like ImageJ)* open access software (https://imagej.net/software/fiji/downloads).

Migration and invasion assays

Melanoma cell motility was investigated by performing 2 types of assays. In the wound healing assay (collective migration assay), B16-F10 mouse melanoma cells (7 × 10^4 cells/cm^2) were grown to confluence in 6-wells plates in complete RPMI medium. Cell monolayers were then washed and incubated for 2 h with mitomycin C (5 μg/mL, Sigma-Aldrich/Merck). After washing the wells twice, cell monolayers were lesioned with a P1000 sterile plastic tip and then incubated with RPMI supplemented with 2% FCS, containing FucSulf1 or heparin (both at 100 μg/mL), for 72 h. Images were captured with an inverted optical microscope in 3 different fields/condition and quantified with the Image J program. In the invasion assay, 8 μm clear porous inserts in 24-well plates were coated with 200 μg/mL of reduced growth factor Matrigel (Corning, cat#354230), diluted in TBS buffer (10 mM Tris, pH 8.0, containing 0.7% NaCl), for 2 h at 37°C. Then, MV3 cells (1.5 × 10^4 cells/cm^2) were seeded on the polymerized matrix in the presence of FucSulf2 or heparin (100 μg/mL), diluted in culture medium. The lower compartment of wells received culture medium supplemented with 5% FCS. After 18 h, cells were removed from the upper side of the filter with the aid of cotton swabs and the inserts were fixed with 3.7% formaldehyde. Cells were labeled with

DAPI and counted with the aid of an EVOS-*fl* fluorescence microscope at ×20 magnification, in 10 representative fields per condition.

In vivo tumor growth assay

B16-F10 cells (2×10^5) were subcutaneously inoculated into the right flank of ketamine/xylazin-anesthetized C57/BL6 mice. Animals were daily treated with intraperitoneal injection of 50 μL of sterile PBS or polysaccharides (4 mg/kg). Tumor volume (V) was accessed by using a caliper for measuring the 2 major diameters (d1 and d2) every 2 days after they were palpable, throughout 20 days of experiment by the formula:

$$V = \frac{\pi (d_1 \times d_2)^2}{6}$$

All experimental procedures were approved by the independent review committee and conducted in accordance with the institutional guidelines of *Universidade Federal do Rio de Janeiro (Centro de Ciências da Saúde/CCS, UFRJ)* for the use of animals in experimental procedures. Since the goals of this experiment did not include the calculation of survival and mortality rates under the different treatments, the experimental endpoint was limited to 20 days after the unexpected death of control animals in the first experiment, to avoid any additional, unnecessary animal suffering. After sacrificing the animals, tumors were removed, weighed on a precision balance in cryotubes and directly frozen on dry ice. Tumors were kept at −80°C until further use. The analysis of protein expression and/or activation by western blotting can be found elsewhere (Section 2.6 and *Supplementary Methods and Data File*).

Statistical analysis

Statistical analyses were performed using the GraphPad Prism software version 7.03 (La Jolla, CA). Data were checked for normal distribution. One-, 2-, or 3-way analysis of variance (ANOVA) was performed, with appropriate post hoc multiple comparisons tests, according to the experimental design, as follows: (i) data sets from time-course proliferation assays aiming to compare concentration effects were analyzed by the 3-way ANOVA, followed by the Tukey's post hoc test, (ii) data from other time-course experiments, such as proliferation and motility assays, and from tumor growth in vivo assays, were analyzed by the 2-way ANOVA and the Tukey's post hoc test, (iii) for all other data sets, comparisons among continuous variables were performed with the ordinary 1-way ANOVA followed by the Dunnetts's post hoc test, and (iv) finally, comparisons between 2 samples were performed using paired or unpaired Student's *t*-test. All values are reported as the mean ± SD, and overall *P*-values < 0.05 were considered as significant, using data from at least 5 independent experiments, unless otherwise indicated in the figure's captions.

Author contributions

Antonio G.F. Lima (Conceptualization-Supporting, Data curation-Equal, Formal analysis-Supporting, Investigation-Equal, Methodology-Equal, Writing—original draft-Supporting), Viviane W. Mignone (Conceptualization-Supporting, Data curation-Equal, Formal analysis-Supporting, Investigation-Equal, Methodology-Equal, Writing—original draft-Supporting), Francisco Vardiero (Investigation-Supporting), Eliene O. Kozlowski (Investigation-Supporting, Methodology-Supporting), Juliana M. Motta (Investigation-Supporting), Laila Ribeiro Fernandes (Investigation-Supporting), Camila C. Figueiredo (Conceptualization-Supporting, Formal analysis-Supporting, Methodology-Supporting), Mauro S.G. Pavão (Formal analysis-Supporting, Methodology-Supporting), Paulo A.S. Mourão (Conceptualization-Lead, Formal analysis-Supporting, Funding acquisition-Equal, Methodology-Supporting, Writing—original draft-Supporting, Writing—review & editing-Supporting), and Verônica Morandi (Conceptualization-Lead, Data curation-Equal, Formal analysis-Lead, Funding acquisition-Equal, Investigation-Supporting, Methodology-Lead, Project administration-Lead, Supervision-Lead, Writing—original draft-Lead, Writing—review & editing-Lead

Acknowledgments

This manuscript is dedicated to the memory of our dearest colleague Eliene O. Kozlowski.

Author contributions

AGFL and VWM performed most of the experiments; AGFL analyzed the results, and revised the manuscript with VM; EOK and MP designed and conducted in vivo experiments with FucSulf1; FV performed the confocal experiments with VM, analyzed data and prepared most of the microscopy images; JMM performed the FucSulf2 in vivo experiments with AGFL; LRF performed cytometric analyses; CCF contributed to the conception of the project, and designed part of the experiments; PM contributed to the overall design of the research, to the analysis of the results and to the final revision of the manuscript; VM conceived the project, performed confocal and blotting experiments with FV, analyzed the data and wrote most of the manuscript.

Funding

The following organisms provided financial support: (i) National Council for Scientific and Technology Development—CNPq/Ministry of Science, Technology and Innovation, Brazil, grants 315831/2020-0 and 312630/2019-0, (ii) Foundation for the Support of Scientific Research of the State of Rio de Janeiro (FAPERJ), Rio de Janeiro State Government, grants E-26/010.002982/2014 and E-26/010.002423/2019, and (iii) National Institutes for Science and Technology (INCT) for Cancer Control (under the lead of the Brazilian National Cancer Institute—INCA). This study was also financed by scholarships from the Coordination for the Improvement of Higher Education Personnel (CAPES)—Brazil.

Conflict of interest statement: None declared.

Data availability

The data that support the findings of this study are available from the corresponding author, V. Morandi, upon reasonable request.

References

Alves AP, Mulloy B, Diniz JA, Mourão PA. Sulfated polysaccharides from the egg jelly layer are species-specific inducers of acrosomal reaction in sperms of sea urchins. *J Biol Chem*. 1997:**272**(11): 6965–6971.

Alves TR, da Fonseca AC, Nunes SS, da Silva AO, Dubois LG, Faria J, Kahn SA, Viana NB, Marcondes J, Legrand C, Moura-Neto

V, Morandi V. Tenascin-C in the extracellular matrix promotes the selection of highly proliferative and tubulogenesis-defective endothelial cells. *Exp Cell Res*. 2011:**317**(15):2073–2085.

Atallah J, Khachfe HH, Berro J, Assi HI. The use of heparin and heparin-like molecules in cancer treatment: a review. *Cancer Treat Res Commun*. 2020:**24**:100192.

Bendas G, Borsig L. Cancer cell adhesion and metastasis: selectins, integrins, and the inhibitory potential of heparins. *Int J Cell Biol*. 2012:**2012**:676731.

Bendas G, Borsig L. Heparanase in cancer metastasis - heparin as a potential inhibitor of cell adhesion molecules. *Adv Exp Med Biol*. 2020:**1221**:309–329.

Borsig L, Wang L, Cavalcante MC, Cardilo-Reis L, Ferreira PL, Mourão PA, Esko JD, Pavão MS. Selectin blocking activity of a fucosylated chondroitin sulfate glycosaminoglycan from sea cucumber. Effect on tumor metastasis and neutrophil recruitment. *J Biol Chem*. 2007:**282**(20):14984–14991.

Braicu C, Buse M, Busuioc C, Drula R, Gulei D, Raduly L, Rusu A, Irimie A, Atanasov AG, Slaby O, et al. A comprehensive review on MAPK: a promising therapeutic target in cancer. *Cancers*. 2019:**11**(10):1618.

Carragher NO, Levkau B, Ross R, Raines EW. Degraded collagen fragments promote rapid disassembly of smooth muscle focal adhesions that correlates with cleavage of pp125(FAK), paxillin, and talin. *J Cell Biol*. 1999:**147**(3):619–630.

Castro MO, Pomin VH, Santos LL, Vilela-Silva AC, Hirohashi N, Pol-Fachin L, Verli H, Mourão PA. A unique 2-sulfated {beta}-galactan from the egg jelly of the sea urchin *Glyptocidaris crenularis*: conformation flexibility versus induction of the sperm acrosome reaction. *J Biol Chem*. 2009:**284**(28):18790–18800.

Casu B, Vlodavsky I, Sanderson RD. Non-anticoagulant heparins and inhibition of cancer. *Pathophysiol Haemost Thromb*. 2008:**36**(3–4): 195–203.

Chaudhary B, Khaled YS, Ammori BJ, Elkord E. Neuropilin 1: function and therapeutic potential in cancer. *Cancer Immunol Immunother*. 2014:**63**(2):81–99.

Chen L, Miao W, Zhang H, Zeng F, Cao C, Qiu R, Yang J, Luo F, Yan J, Lv H, et al. The inhibitory effects of a monoclonal antibody targeting neuropilin-1 on adhesion of glioma cells to fibronectin. *J Biomed Nanotechnol*. 2014:**10**(11):3373–3380.

Cromm PM, Samarasinghe KTG, Hines J, Crews CM. Addressing kinase-independent functions of Fak via PROTAC-mediated degradation. *J Am Chem Soc*. 2018:**140**(49):17019–17026.

Dawson JC, Serrels A, Stupack DG, Schlaepfer DD, Frame MC. Targeting FAK in anticancer combination therapies. *Nat Rev Cancer*. 2021:**21**(5):313–324.

Disanza A, Bisi S, Frittoli E, Malinverno C, Marchesi S, Palamidessi A, Rizvi A, Scita G. Is cell migration a selectable trait in the natural evolution of cancer development? *Philos Trans R Soc Lond Ser B Biol Sci*. 2019:**374**(1779):20180224.

Fonseca RJ, Oliveira SN, Pomin VH, Mecawi AS, Araujo IG, Mourão PA. Effects of oversulfated and fucosylated chondroitin sulfates on coagulation. Challenges for the study of anticoagulant polysaccharides. *Thromb Haemost*. 2010:**103**(5):994–1004.

de Franceschi N, Hamidi H, Alanko J, Sahgal P, Ivaska J. Integrin traffic - the update. *J Cell Sci*. 2015:**128**(5):839–852.

Fukasawa M, Matsushita A, Korc M. Neuropilin-1 interacts with integrin beta1 and modulates pancreatic cancer cell growth, survival and invasion. *Cancer Biol Ther*. 2007:**6**(8): 1173–1180.

Glauser BF, Mourão PAS, Pomin VH. Marine sulfated glycans with serpin-unrelated anticoagulant properties. *Advances Clin Ther*. 2013:**62**:269–303.

Gockel LM, Heyes M, Li H, Al Nahain A, Gorzelanny C, Schlesinger M, Holdenrieder S, Li JP, Ferro V, Bendas G. Inhibition of tumor-host cell interactions using synthetic heparin mimetics. *ACS Appl Mater Interfaces*. 2021:**13**(6):7080–7093.

Goel HL, Mercurio AM. VEGF targets the tumour cell. *Nat Rev Cancer*. 2013:**13**(12):871–882.

Graziani G, Lacal PM. Neuropilin-1 as therapeutic target for malignant melanoma. *Front Oncol*. 2015:**5**:125.

Griggs LA, Hassan NT, Malik RS, Griffin BP, Martinez BA, Elmore LW, Lemmon CA. Fibronectin fibrils regulate TGF-β1-induced epithelial-mesenchymal transition. *Matrix Biol*. 2017:**60-61**: 157–175.

Guo HF, Vander Kooi CW. Neuropilin functions as an essential cell surface receptor. *J Biol Chem*. 2015:**290**(49):29120–29126.

Hanahan D, Weinberg RA. Hallmarks of cancer: the next generation. *Cell*. 2011:**144**(5):646–674.

Hess AR, Hendrix MJ. Focal adhesion kinase signaling and the aggressive melanoma phenotype. *Cell Cycle*. 2006:**5**(5):478–480.

Hill KE, Lovett BM, Schwarzbauer JE. Heparan sulfate is necessary for the early formation of nascent fibronectin and collagen I fibrils at matrix assembly sites. *J Biol Chem*. 2022:**298**(1):101479.

Hynes RO, Destree AT, Perkins ME, Wagner DD. Cell surface fibronectin and oncogenic transformation. *J Supramol Struct*. 1979:**11**(1):95–104.

Hytönen VP, Wehrle-Haller B. Mechanosensing in cell-matrix adhesions - converting tension into chemical signals. *Exp Cell Res*. 2015:**343**(1):35–41.

Kalluri R, Weinberg RA. The basics of epithelial-mesenchymal transition. *J Clin Invest*. 2009:**119**(6):1420–1428.

Khanna C, Hunter K. Modeling metastasis *in vivo*. *Carcinogenesis*. 2005:**26**(3):513–523.

Kuderer NM, Khorana AA, Lyman GH, Francis CW. A meta-analysis and systematic review of the efficacy and safety of anticoagulants as cancer treatment: impact on survival and bleeding complications. *Cancer*. 2007:**110**(5):1149–1161.

LaFlamme SE, Shi F, Sottile J. Integrin trafficking. In: LaFlamme SE, Kowalczyk AP, editors. *Cell junctions*. Weinheim (DE): Wiley-VCH; 2008. pp. 89–107

Lee AY, Peterson EA. Treatment of cancer-associated thrombosis. *Blood*. 2013:**122**(14):2310–2317.

Li Y, Lovett D, Zhang Q, Neelam S, Kuchibhotla RA, Zhu R, Gundersen GG, Lele TP, Dickinson RB. Moving cell boundaries drive nuclear shaping during cell spreading. *Biophys J*. 2015:**109**(4): 670–686.

Ma SN, Mao ZX, Wu Y, Liang MX, Wang DD, Chen X, Chang PA, Zhang W, Tang JH. The anti-cancer properties of heparin and its derivatives: a review and prospect. *Cell Adhes Migr*. 2020:**14**(1): 118–128.

Manning BD, Toker A. AKT/PKB Signaling: navigating the network. *Cell*. 2017:**169**(3):381–405.

Miller MA, Sullivan RJ, Lauffenburger DA. Molecular pathways: receptor ectodomain shedding in treatment, resistance, and monitoring of cancer. *Clin Cancer Res*. 2017:**23**(3):623–629.

Morandi V, Cherradi SE, Lambert S, Fauvel-Lafève F, Legrand YJ, Legrand C. Proinflammatory cytokines (interleukin-1 beta and tumor necrosis factor-alpha) down regulate synthesis and secretion of thrombospondin by human endothelial cells. *J Cell Physiol*. 1994:**160**(2):367–377.

van Muijen GN, Jansen KF, Cornelissen IM, Smeets DF, Beck JL, Ruiter DJ. Establishment and characterization of a human melanoma cell line (MV3) which is highly metastatic in nude mice. *Int J Cancer*. 1991:**48**(1):85–91.

Mulloy B, Ribeiro AC, Alves AP, Vieira RP, Mourão PA. Sulfated fucans from echinoderms have a regular tetrasaccharide repeating unit defined by specific patterns of sulfation at the 0-2 and 0-4 positions. *J Biol Chem*. 1994:**269**(35):22113–22123.

Namekawa T, Ikeda K, Horie-Inoue K, Inoue S. Application of prostate cancer models for preclinical study: advantages and limitations of cell lines, patient-derived xenografts, and three-dimensional culture of patient-derived cells. *Cell*. 2019:**8**(1):74.

Pereira MS, Mulloy B, Mourão PA. Structure and anticoagulant activity of sulfated fucans. Comparison between the regular, repetitive, and linear fucans from echinoderms with the more heterogeneous and branched polymers from brown algae. *J Biol Chem*. 1999:**274**(12): 7656–7667.

Pomin VH, Mourão PA. Specific sulfation and glycosylation-a structural combination for the anticoagulation of marine carbohydrates. *Front Cell Infect Microbiol*. 2014:**4**:33.

Queiroz IN, Wang X, Glushka JN, Santos GR, Valente AP, Prestegard JH, Woods RJ, Mourão PA, Pomin VH. Impact of sulfation pattern on the conformation and dynamics of sulfated fucan oligosaccharides as revealed by NMR and MD. *Glycobiology*. 2015:**25**(5): 535–547.

Razak NBA, Jones G, Bhandari M, Berndt MC, Metharom P. Cancer-associated thrombosis: an overview of mechanisms, risk factors, and treatment. *Cancers*. 2018:**10**(10):380.

Regad T. Targeting RTK Signaling pathways in cancer. *Cancers*. 2015:**7**(3):1758–1784.

Ribeiro AC, Vieira RP, Mourão PA, Mulloy B. A sulfated alpha-L-fucan from sea cucumber. *Carbohydr Res*. 1994:**255**:225–240.

Schwartz MA, Assoian RK. Integrins and cell proliferation: regulation of cyclin-dependent kinases via cytoplasmic signaling pathways. *J Cell Sci*. 2001:**114**(14):2553–2560.

Sczekan MM, Juliano RL. Internalization of the fibronectin receptor is a constitutive process. *J Cell Physiol*. 1990:**142**(3):574–580.

Sechler JL, Schwarzbauer JE. Control of cell cycle progression by fibronectin matrix architecture. *J Biol Chem*. 1998:**273**(40): 25533–25536.

Sosa MS, Bragado P, Aquirre-Ghiso JA. Mechanisms of disseminated cancer cell dormancy: an awakening field. *Nat Rev Cancer*. 2014:**14**(9):611–622.

Sottile J, Hocking DC, Swiatek PJ. Fibronectin matrix assembly enhances adhesion-dependent cell growth. *J Cell Sci*. 1998:**111**(19): 2933–2943.

Spada S, Tocci A, Di Modugno F, Nisticò P. Fibronectin as a multiregulatory molecule crucial in tumor matrisome: from structural and functional features to clinical practice in oncology. *J Exp Clin Cancer Res*. 2021:**40**(1):102.

Sulzmaier FJ, Jean C, Schlaepfer DD. FAK in cancer: mechanistic findings and clinical applications. *Nat Rev Cancer*. 2014:**14**(9): 598–610.

Valdembri D, Caswell PT, Anderson KI, Schwarz JP, König I, Astanina E, Caccavari F, Norman JC, Humphries MJ, Bussolino F, et al. Neuropilin-1/GIPC1 signaling regulates alpha5beta1 integrin traffic and function in endothelial cells. *PLoS Biol*. 2009: 7(1):e25.

Varki A, Cummings RD, Aebi M, Packer NH, Seeberger PH, Esko JD, et al. Symbol nomenclature for graphical representations of glycans. *Glycobiology*. 2015:**25**(12):1323–1324.

Woods A, Longley RL, Tumova S, Couchman JR. Syndecan-4 binding to the high affinity heparin-binding domain of fibronectin drives focal adhesion formation in fibroblasts. *Arch Biochem Biophys*. 2000:**374**(1):66–72.

Xie M, Li JP. Heparan sulfate proteoglycan - a common receptor for diverse cytokines. *Cell Signal*. 2019:**54**:115–121.

Yan L, Moses MA, Huang S, Ingber DE. Adhesion-dependent control of matrix metalloproteinase-2 activation in human capillary endothelial cells. *J Cell Sci*. 2000:**113**(22):3979–3987.n.

Yaqoob U, Cao S, Shergill U, Jagavelu K, Geng Z, Yin M, de Assuncao TM, Cao Y, Szabolcs A, Thorgeirsson S, et al. Neuropilin-1 stimulates tumor growth by increasing fibronectin fibril assembly in the tumor microenvironment. *Cancer Res*. 2012:**72**(16): 4047–4059.

Zeng F, Luo F, Lv S, Zhang H, Cao C, Chen X, Wang S, Li Z, Wang X, Dou X, et al. A monoclonal antibody targeting neuropilin-1 inhibits adhesion of MCF7 breast cancer cells to fibronectin by suppressing the FAK/p130cas signaling pathway. *Anti-Cancer Drugs*. 2014:**25**(6):663–672.

Zhao X, Guan JL. Focal adhesion kinase and its signaling pathways in cell migration and angiogenesis. *Adv Drug Deliv Rev*. 2011:**63**(8): 610–615.